JOURNAL OF GEOPHYSICAL RESEARCH, VOL. 114, D02113, doi:10.1029/2008JD010578, 2009

Interpreting ^{10}Be changes during the Maunder Minimum

Christy V. Field,[1,2] Gavin A. Schmidt,[3] and Drew T. Shindell[3]

Received 10 June 2008; revised 5 September 2008; accepted 11 November 2008; published 29 January 2009.

[1] Beryllium-10 archives are important resources for understanding how solar activity may have varied in the past. Climate simulations using the Goddard Institute for Space Studies ModelE general circulation model are used to calibrate the impacts of production changes, solar forcings, and volcanic aerosol forcing on ^{10}Be concentration during periods such as the Maunder Minimum (1645–1715 A.D.). We find that for the preindustrial period, production-related ^{10}Be changes are the dominant signal in snow concentration, and that the effects of both solar and volcanic forcings on climate are relatively minor. Ambiguities in determining the observed changes in ^{10}Be snow concentration during the Maunder Minimum complicate the process of estimating changes in the solar modulation strength during that time. Given those limitations, we estimate that the average value of the solar modulation parameter ϕ was between 280 and 395 MeV over the course of the Maunder Minimum, and was approximately 142 MeV during the years of peak ^{10}Be concentration as recorded in the Dye 3 and South Pole ice core records.

Citation: Field, C. V., G. A. Schmidt, and D. T. Shindell (2009), Interpreting ^{10}Be changes during the Maunder Minimum, *J. Geophys. Res.*, *114*, D02113, doi:10.1029/2008JD010578.

1. Introduction

[2] As the study of present-day climate change continues to evolve, so does the need to develop a more comprehensive understanding of natural climate forcings, including changes in solar irradiance. The variations in solar output associated with the 11-year sunspot cycle do not seem to have a strong impact on surface climate, however the so-called "Grand Minima," periods of prolonged quiescence in solar activity which appear to have taken place several times during the past 1000 years, may have had a greater impact [*McCracken et al.*, 2004]. One of the more recent and pronounced of these periods, the Maunder Minimum (MM), occurred from 1645 to 1715 A.D. [*Eddy*, 1976; *Stuiver and Quay*, 1980; *Ribes and Nesme-Ribes*, 1993; *Lean*, 2000] and was characterized by very low sunspot numbers [*Hoyt and Schatten*, 1998], which has been assumed to imply a reduction in solar irradiance (of uncertain magnitude) [*Willson and Hudson*, 1988; *Radick et al.*, 1990; *Foukal et al.*, 2006]. The reduced solar activity during the MM also coincided with a period of reduced temperatures, increased volcanic activity and glacial expansion in the northern hemisphere [*Overpeck et al.*, 2004; *Jones et al.*, 1998; *Jones and Mann*, 2004; *Crowley*, 2000; *Crowley et al.*, 2008; *Free and Robock*, 1999], particularly during the late MM (approximately 1680–1710).

[3] Only satellite data provide direct observations of changes in solar irradiance, but since such observations are not available during any of the Grand Minima, we must turn to proxy indicators. Cosmogenic isotopes such as beryllium-10 (^{10}Be) are particularly useful in this regard, since their production by high-energy galactic cosmic rays (GCR) is modulated by the strength of the solar magnetic field [*Lal and Peters*, 1967; *Masarik and Beer*, 1999]. (Changes in geomagnetic field strength also affect GCR flux, but generally on much longer timescales than the decadal or centennial changes associated with solar activity [*Muscheler et al.*, 2007].) The production of cosmogenic isotopes takes place mainly in the stratosphere and upper troposphere, and is the result of spallation reactions between cosmic ray particles and atmospheric oxygen and nitrogen [*Lal and Peters*, 1967; *McHargue and Damon*, 1991]. Increases in solar magnetic activity, which are correlated with increases in solar irradiance over the 11-year sunspot cycle [*Lean*, 1994; *Lean et al.*, 2002], cause Earth's atmosphere to be more strongly shielded from the GCR flux. Such shielding, typically described using the solar modulation parameter ϕ [*Gleeson and Axford*, 1968], results in lower levels of cosmogenic isotope production [*Masarik and Beer*, 1999; *Stuiver and Quay*, 1980; *McCracken et al.*, 2004]. This inverse relationship is consistent with the relatively high concentration of ^{10}Be stored in ice core archives during the MM (Figure 1), when sunspot activity was persistently low, and also suggests that reduced solar irradiance may have contributed to the colder conditions during the MM [*Eddy*, 1976].

[4] The excellent time resolution available with ice-core records makes ^{10}Be data from Greenland and Antarctica the

[1]Department of Earth and Environmental Sciences, Columbia University, New York, New York, USA.
[2]NASA Goddard Institute for Space Studies, New York, New York, USA.
[3]NASA Goddard Institute for Space Studies and Center for Climate Systems Research, Columbia University, New York, New York, USA.

0148-0227/09/2008JD010578$09.00

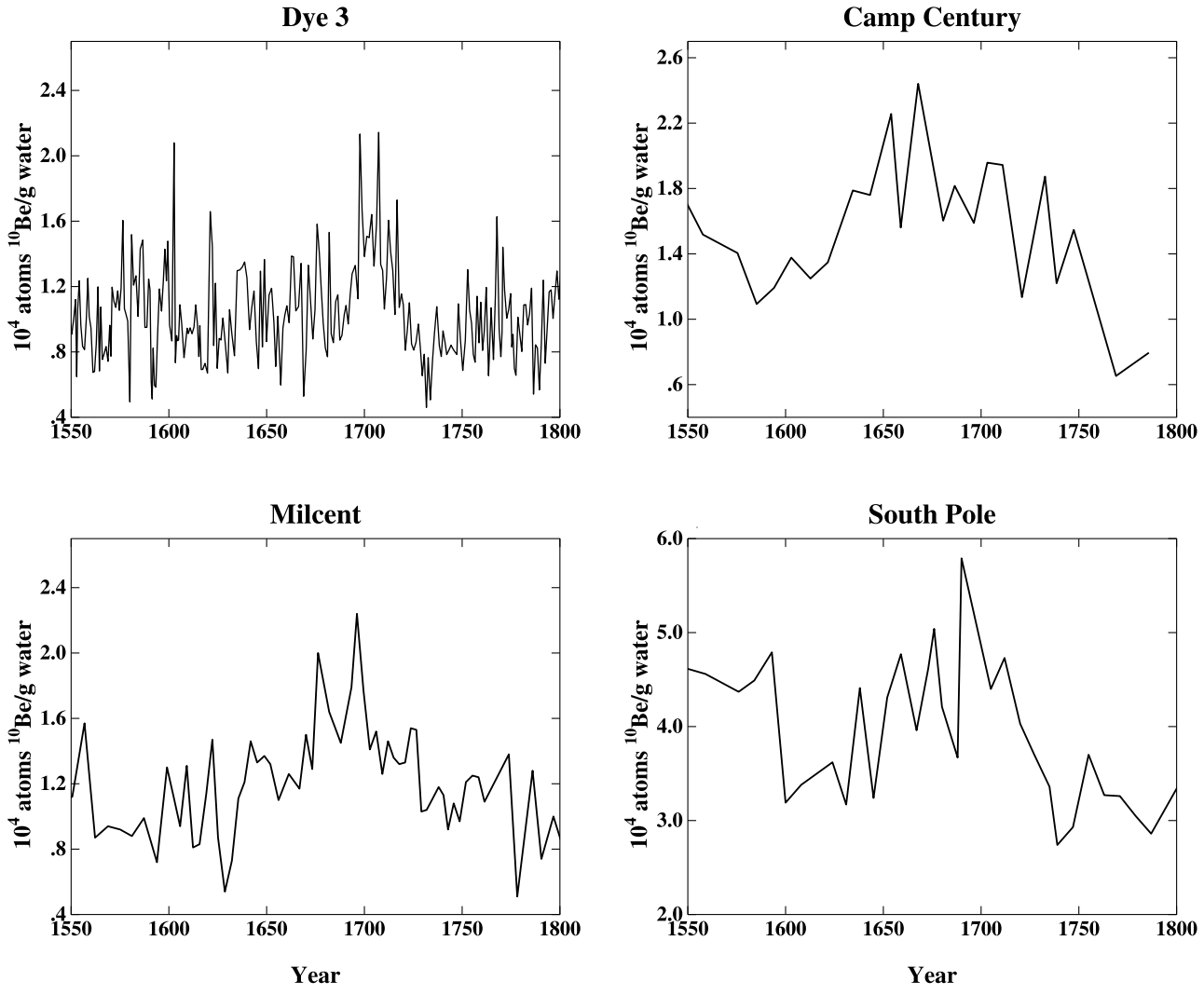

Figure 1. The ^{10}Be snow concentration at ice-core locations for 1550–1800. Data are from *Beer et al.* [1990] (Dye 3), *Beer et al.* [1988] (Camp Century), *Beer et al.* [1983] (Milcent), and *Raisbeck et al.* [1990] (South Pole).

preferred archives for estimating solar changes over the entire Holocene. There are, however, potential complications when interpreting ^{10}Be records. In ice cores, ^{10}Be is primarily measured in terms of its concentration per gram of snow water equivalent. Changes in climate (which may affect wet deposition, dry deposition, atmospheric transport and precipitation, and which may occur independently of changes in solar irradiance) and changes in ^{10}Be production therefore both play a role in determining ^{10}Be snow concentrations. For instance, if reduced snowfall and increased ^{10}Be production occur simultaneously, the ^{10}Be concentrations in the ice-core record will be higher than they would be owing to changes in production alone [*Field et al.*, 2006; *LeGrande et al.*, 2006]. Under such circumstances it could be possible to infer larger changes in solar magnetic activity and GCR shielding than actually took place.

[5] Disentangling solar- and climate-related impacts on ^{10}Be ice-core records is particularly relevant for understanding total solar irradiance (TSI) changes during the Maunder Minimum. The coincidence of such a prolonged solar anomaly with a well-documented period of northern hemisphere cooling; the timing of these events prior to the onset of anthropogenic climate change; the recent invention of the telescope and hence the abundance of sunspot observations during the MM; and the existence of several sets of ^{10}Be data spanning the time period collectively provide a rich set of resources for interpreting not only how irradiance changes impact Earth's climate, but also how climate changes and production changes are expressed in ^{10}Be ice core records.

[6] General circulation models have the capability to play a key role in answering these questions since they provide the opportunity to vary climate and ^{10}Be production independently. During the MM, the relevant climate forcings are from the cooling effects of stratospheric aerosols due to increased levels of volcanic activity, and from direct and indirect changes associated with reduced TSI. In addition to the direct TSI change, capturing the variability in the UV bands is also important. Satellite observations have shown that changes in solar UV radiation are significantly larger in percentage terms than changes in the visible spectrum [*Lean*, 1994; *Lean et al.*, 1995]. They affect the distribution of stratospheric ozone over the course of the sunspot cycle

Table 1. Maunder Minimum Experiments

Run	TSI (W/m^2)	Percent Change From 1979	Additional Forcing
Solar maximum (Sx), 1979	1366.68	-	
1 × solar minimum (1Sn), 1986	1365.65	0.075	
2 × solar minimum (2Sn), 1912	1364.57	0.15	
3 × solar minimum (3Sn)	1363.59	0.23	
4 × solar minimum (4Sn)	1362.56	0.30	
Volcanic runs			
0SnV, 1979	1366.68	-	−0.16 W/m^2 stratospheric aerosol forcing
1SnV, 1986	1365.65	0.075	same as above
2SnV, 1912	1364.57	0.15	same as above

and can significantly change the vertical temperature profile, particularly at low latitudes [*Haigh*, 1996; *Shindell et al.*, 2006a]. The temperature changes may in turn affect the propagation of planetary wave energy and can impact surface temperature and storminess at high latitudes [*Shindell et al.*, 1999b, 2001; *Rind et al.*, 2007]. The effect of these changes on storm track patterns is another mechanism by which solar-induced climate change might affect the ^{10}Be record.

[7] In this paper, we vary TSI, ozone, spectral irradiance, stratospheric volcanic aerosols and ^{10}Be production rates to present a suite of climate simulations spanning a range of possible MM scenarios. We then examine how the modeled changes in climate and production affect ^{10}Be at different ice-core locations, and how our results compare with the observational record.

2. GISS ModelE Description

[8] Our experiments were performed using the latest version of the Goddard Institute for Space Studies (GISS) ModelE general circulation model (GCM) [*Schmidt et al.*, 2006]. This version of the model has a horizontal resolution of 4° × 5° (latitude × longitude) and a vertical resolution of 23 layers. The model top is at 0.002 mbar, which allows us to simulate the full stratosphere. This degree of stratospheric resolution is important, as previous studies have shown that models without a full stratosphere may misrepresent stratosphere-troposphere exchange (STE), a significant consideration in this case as approximately half of all ^{10}Be is produced in the stratosphere. Also, models with limited representations of the stratosphere have been shown to be less skilled at simulating lower stratospheric variability than models with higher-pressure boundaries [*Rind et al.*, 1999]. The formulation for the gravity wave drag is slightly changed from that of *Schmidt et al.* [2006] to allow for improved stratospheric circulation and STE. In general, GCMs tend to have levels of STE that are higher than the observed values, and, correspondingly, younger ages of stratospheric air. While the age of air in ModelE's stratosphere also somewhat younger than observations [*Rind et al.*, 2007], it is well simulated in comparison to other GCMs [*Shindell et al.*, 2006b].

[9] In all runs, we used the calculated cosmogenic production functions from *Masarik and Beer* [1999] (see *Field et al.* [2006, Figure 1] for climatological plots of wet and dry ^{10}Be deposition). All tracers in the model (including ^{10}Be) are subject to the advection, mixing and convection processes consistent with the model air mass fluxes. We assume that there are always sufficient sulfate aerosols available to scavenge the ^{10}Be, and that beryllium isotopes attach to sulfate aerosols immediately after production and are 100% soluble. Aerosol gravitational settling is included, and in stratiform and convective clouds, aerosol species are transported, dissolved, evaporated and scavenged according to processes for each cloud type. The model also allows for faster settling of fine aerosols in the stratosphere, where the mean free path exceeds the particle radius [*Koch and Rind*, 1998].

[10] In the boundary conditions near the surface, ^{10}Be is handled using the same turbulent exchange coefficients as the model humidity. The dry deposition scheme, which is based on the resistance-in-series scheme described by *Wesely and Hicks* [1977] derived from the Harvard GISS chemical transport model [e.g., *Chin et al.*, 1996], is fully coupled to the GCM processes and makes use of the GCM-assumed leaf area indices, surface types, radiation, boundary layer height, Monin-Obhukov length, etc. [*Koch et al.*, 2006].

3. Experimental Design

[11] To simulate the climate changes that might have taken place during the MM, we performed a suite of model runs to capture a range of possible solar forcings, volcanic changes and climate responses. The different experiments are summarized in Table 1. The yardstick for our solar forcing was the spectral and TSI changes between a present-day solar maximum and solar minimum (1979 and 1986 respectively). As neither the relationship between sunspot number and TSI nor between cosmogenic isotopes and TSI are well known, estimates for how much solar irradiance might have decreased during the Maunder Minimum vary widely, ranging from 0.05% to 0.5% [*Hoyt and Schatten*, 1993; *Lean et al.*, 1995; *Lean*, 2000]. To address this uncertainty, we performed four sets of experiments to simulate what the solar-related impact on ice-core ^{10}Be would be like for a ΔTSI equivalent in magnitude to 1, 2, 3, and 4 times the change from 1979 to 1986. The ΔTSI from 1979 to 1986 is 0.075%, which places our 1 × ΔTSI experiments at the low end of the estimated MM range [*Foukal et al.*, 2006]. We simulate the 2 × ΔTSI scenario using data from 1912 (TSI = 1364.57 W/m^2, about a 0.15% change from 1979) [*Lean et al.*, 2002].

[12] To simulate the 3 × ΔTSI and 4 × ΔTSI scenarios, we calculated the 1979-to-1986 changes for TSI, tripled and quadrupled them, and forced the model with the resulting changes. The same process was also applied to the three UV

Table 2. Model Results: Surface Air Temperature Changes, Relative to Sx Run[a]

Run	Global Mean	Northern Hemisphere	Northern Hemisphere Land	Europe, Winter
1Sn	−0.14	−0.12	−0.15	−0.15
2Sn	−0.21	−0.24	−0.26	−0.30
3Sn	−0.30	−0.31	−0.38	−0.41
4Sn	−0.44	−0.45	−0.55	−0.53
0SnV	−0.12	−0.11	−0.16	−0.16
1SnV	−0.21	−0.21	−0.27	−0.22
2SnV	−0.31	−0.32	−0.40	−0.30

[a]Unit is °C.

wavelength bands in the GCM (100–295 nm, 295–310 nm, and 310–366 nm) that affect stratospheric ozone in the model, giving an enhanced UV variability compared to the changes in TSI. For the different amounts of UV changes, ozone concentrations are prescribed according to the results of previous model experiments involving fully coupled ozone chemistry [*Shindell et al.*, 2006a]. Over the UV bands, the radiation changes range from 0.5% to 5.2% for the 3 × ΔTSI and 4 × ΔTSI runs, with greater variability at the shorter wavelengths.

[13] For the control scenario, we set ^{10}Be production equal to what it would be for ϕ = 700 MeV, which is the approximate midpoint for solar modulation between present-day solar maxima and minima [*Masarik and Beer*, 1999]. To simulate the increased production expected during the MM, we ran the model with ϕ = 500 MeV (the approximate value observed during recent solar minima) and also with ϕ = 100 MeV, which is comparable to the MM production value estimated by *McCracken et al.* [2004] using ^{10}Be records from Dye 3 and South Pole (ϕ = 84 MeV); to the average value from 1645–1715 (ϕ = 127 MeV) estimated from ^{14}C data by *Muscheler et al.* [2007]; to the value estimated by *Vonmoos et al.* [2006] using ^{10}Be from the GRIP ice core (ϕ = approximately 200 MeV); and to the value estimated by *Steinhilber et al.* [2008] on the basis of a composite of three ϕ reconstructions (ϕ = approximately 290 MeV).

[14] Along with solar changes, volcanic eruptions were also an important climate forcing in the preindustrial period. We performed an additional set of experiments to assess the possible impact. According to *Crowley* [2000], the mean negative volcanic forcing between 1660 and 1690 was about 0.16 W/m^2 compared to a century later. To simulate the combined effect of volcanism and TSI changes, we ran the model with a constant stratospheric aerosol radiative forcing of −0.16 W/m^2 and ϕ = 100 MeV. We performed these volcanic simulations with TSI values for 1979, 1 × ΔTSI and 2 × ΔTSI. Volcanic aerosol properties are defined as by *Sato et al.* [1993].

[15] For all experiments, we configured the model with a preindustrial atmosphere and a mixed-layer ocean since the multidecadal duration of the MM would make it possible for ocean temperatures to respond to potential irradiance changes. In all simulations, a 20-year spin-up period was used to ensure that equilibrium had been reached for sea surface temperatures and for the atmospheric distribution of cosmogenic isotopes. The results for all experiments were averaged over the 30 years following the spin-up period.

4. Climate Response to Solar Forcing

[16] Reconstructions of northern hemisphere (NH) surface air temperature from various proxies (ice cores, corals, tree rings and other sources) indicate that during the late 17th century, NH temperatures are estimated to have been −0.2 to −0.6° C relative to the 1961–1990 mean value, and from +0.1 to −0.3° C relative to the 1850–1900 mean value [*Jones et al.*, 1998; *Briffa et al.*, 2001; *Mann et al.*, 1999; *Briffa*, 2000; *Overpeck et al.*, 2004; *Crowley and Lowery*, 2000]. In Europe during the same time period, wintertime temperatures are estimated to have been about −0.25°C compared to the 1850–1900 mean [*Luterbacher et al.*, 2004]. We performed our solar maximum simulation with a preindustrial atmosphere in order to avoid the effects of anthropogenic climate change; for this reason; we would expect our simulated cooling to correspond more closely to the reconstructed temperature estimates relative to the 1850–1900 values, as solar forcing is a much larger fraction of the total probable forcing relative to 1850–1900 than it is relative to 1961–1990. The degree of global, NH and European cooling in the different solar minimum runs relative to the solar maximum run is shown in Table 2. The amount of global cooling that takes place in the model is fairly linear with respect to the magnitude of the TSI changes, with approximately 0.11° C of cooling for each multiple of sunspot-cycle forcing. For the global mean and NH temperature changes, all of the simulated values fall within the reconstructed range except for the 4Sn run, which is somewhat cooler; for European wintertime temperatures, both the 3Sn and 4Sn simulations are cooler than the reconstructed estimates. The temperature changes in these experiments are similar to those from other MM modeling experiments, such as those of *Shindell et al.* [2001] (global mean cooling of 0.34°C, driven by solar forcing only, approximately 2 × ΔTSI). The model used by *Shindell et al.* [2001] is an older version than is used here, in particular having lower horizontal resolution (8° × 10°) and older physics. Our temperature changes are also comparable to those given by *Langematz et al.* [2005] (0.86°C cooling for the NH relative to present-day conditions, forced with greenhouse gas changes and irradiance changes of about 2.5 × ΔTSI) and *Heikkilä et al.* [2008] (global mean cooling of 0.7°C relative to the present day, forced with prescribed SSTs, greenhouse gas changes and approximately 1.5 × ΔTSI).

[17] Around the Mediterranean, simulated temperatures stay the same or warm slightly as irradiance decreases. This warming is accompanied by small increases in wintertime precipitation (up to 0.3 mm/d). The combination of warm, moist wintertime conditions around the Mediterranean is indicative of the negative phase of the North Atlantic Oscillation (NAO), the large-scale dipole of atmospheric pressure that acts as the dominant mode of winter climate variability over the North Atlantic. The NAO index is typically defined as the difference in sea-level pressure between Iceland and the Azores, and is described as being in a negative phase when that pressure gradient is lower than usual. Reconstructions of the NAO using ice cores, tree

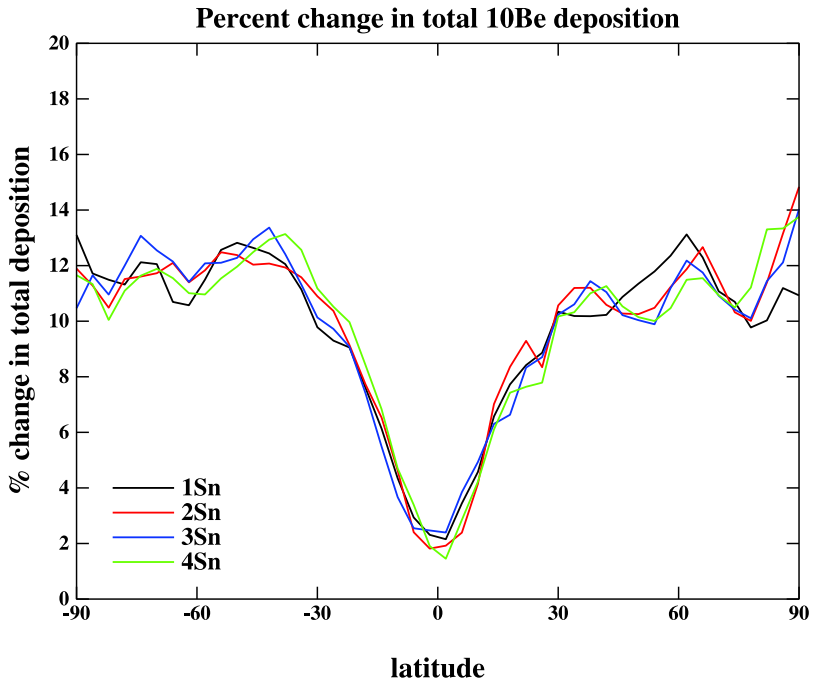

Figure 2. Percent change in zonal mean total deposition of modeled ^{10}Be. All data shown are for runs with ϕ = 500 MeV, relative to the solar maximum run (ϕ = 700 MeV), and all data are 30-year averages. The pattern of change is dominated by the production change, while climate has little impact on the zonal mean deposition.

rings, documentary evidence and other proxies indicate that the NAO index was predominantly negative during the MM [*Luterbacher et al.*, 2004; *Appenzeller et al.*, 1998; *Rodrigo et al.*, 2001]. While differences in model configurations can lead to different degrees of sea level pressure response [*Miller et al.*, 2006; *Palmer et al.*, 2004], previous modeling experiments have shown a sensitivity to NAO changes caused by external forcings [*Shindell et al.*, 1999a, 2001; *Gillett et al.*, 2002]. A comparable response is seen here, with positive sea-level pressure anomalies on the order of 0.8–3.2 mbar over Iceland and negative anomalies of 0.1–1.1 mbar over the Azores for decreasing solar irradiance.

[18] The negative phase of the NAO seen in the model stems in part from the parameterized change in stratospheric ozone associated with the changes in solar irradiance [*Shindell et al.*, 2006a, 2006b]. Because the UV radiation in the solar minimum simulations is reduced, temperatures in the upper stratosphere are cooler, which, combined with the changes in ozone, results in radiative cooling up to 2.4°C in both the upper and lower stratosphere. This cooling reduces the equator-to-pole temperature gradient in the lower stratosphere. A reduction in stability caused by the cooling aloft leads to increased eddy kinetic energy in NH midlatitudes. These changes in eddy energy propagate upward and poleward, causing a reduction in the northward eddy transport of zonal momentum (up to -10 m^2/s^2). This equatorward momentum transport is accompanied by a weakening of the NH zonal winds (up to -2.2 m/s) and an increase in the northward Eliassen-Palm (EP) flux, producing an anomalous EP flux convergence. The EP flux convergence is associated with reduced poleward transport of quasi-geostrophic potential vorticity, implying less positive vorticity at higher latitudes and therefore higher sea-level pressure, which is consistent with the negative NAO seen in the model results [*Shindell et al.*, 2001].

[19] Overall, the model can simulate the approximate degree of cooling and also the NH sea-level pressure changes (associated with the negative phase of the NAO) that are thought to have characterized the climate during the MM. With the exception of the cooling in the 4Sn scenario (which exceeds the estimates of most temperature reconstructions), the range of the estimates for the reconstructed MM temperatures makes it difficult to select a single solar minimum run as a best match for the MM paleodata.

5. Climate Response to Volcanic Forcing

[20] The global, NH and European wintertime cooling for the volcanic runs is shown in Table 2. In the global mean and also for the NH, the volcanic forcing used in these experiments is enough to cause temperature changes of about the same magnitude as a single solar cycle's worth of TSI forcing. For the European wintertime temperatures, the cooling in the 0SnV run is approximately the same as for the 1Sn run (-0.16 versus -0.15), however the cooling in 1SnV and 2SnV is less than the cooling in 2Sn and 3Sn respectively, suggesting that European winter temperatures do not respond linearly to the volcanic forcing used here.

[21] Previous experiments with GISS ModelE have demonstrated that volcanic aerosols lead to a positive phase of the NAO for the winters immediately following an eruption, but also that the effect of reduced TSI dominates when solar forcing and volcanic forcing are applied in tandem, leading to a NH climate response similar to that seen during the late MM [*Shindell et al.*, 2004]. Similarly, in our runs, the phase of the NAO relative to the control is negative in all three

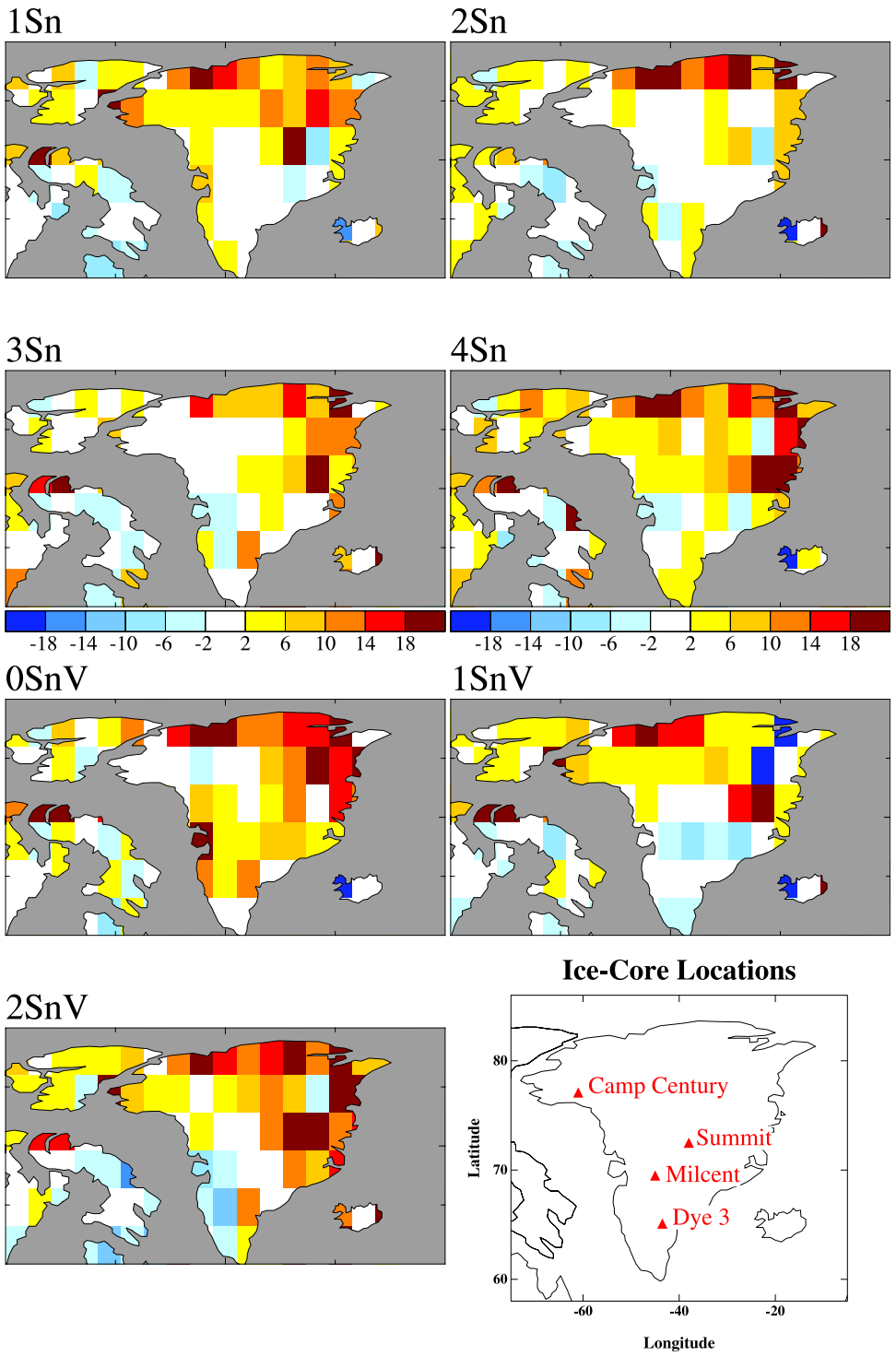

Figure 3. Percent change in modeled ^{10}Be snow concentration due to TSI-related and/or volcanic-related climate changes.

scenarios with volcanic forcing. In the experiments with only solar forcing, atmospheric cooling at low latitudes extends from the troposphere to the stratosphere. In the volcanic runs, the low-latitude cooling is limited to the troposphere, since the aerosols in the stratosphere absorb solar radiation and create moderate warming aloft. However the resulting changes in the latitudinal temperature gradient are sufficient to trigger dynamical changes that are basically the same as those in the solar-only runs, demonstrating the dominance of TSI-related climate changes relative to the effects of moderate, continuous volcanic aerosol forcing.

[22] In these simulations, the cooling associated with volcanic aerosol forcing and also the persistence of a negative phase of the NAO suggest that a range of volcanic and solar changes could have created conditions that match reconstructions of the MM climate. Further data will be

Table 3. Percent Increase in Modeled ^{10}Be Snow Concentration, Experiment Minus Control $\pm 1\sigma$[a]

Run, ϕ	Dye 3	Camp Century	Milcent	Summit	Taylor Dome	South Pole
0Sn, 500	12 ± 3	12 ± 1	12 ± 2	12 ± 1	13 ± 1	13 ± 1
1Sn, 500	10 ± 2	14 ± 1	12 ± 2	15 ± 1	19 ± 2	18 ± 1
2Sn, 500	16 ± 2	14 ± 1	14 ± 2	18 ± 1	14 ± 1	12 ± 1
3Sn, 500	25 ± 3	12 ± 1	12 ± 2	16 ± 1	17 ± 1	18 ± 1
4Sn, 500	16 ± 2	16 ± 1	12 ± 2	22 ± 1	20 ± 1	15 ± 1
0Sn, 100	50 ± 3	50 ± 1	47 ± 2	50 ± 1	52 ± 2	52 ± 1
1Sn, 100	47 ± 3	53 ± 1	47 ± 2	53 ± 1	61 ± 2	59 ± 1
2Sn, 100	55 ± 3	53 ± 1	53 ± 2	57 ± 2	54 ± 2	51 ± 1
3Sn, 100	67 ± 3	50 ± 1	49 ± 2	55 ± 1	57 ± 2	59 ± 1
4Sn, 100	54 ± 3	56 ± 1	49 ± 2	64 ± 2	62 ± 2	54 ± 2
0SnV, 100	65 ± 3	52 ± 1	57 ± 2	58 ± 2	69 ± 1	42 ± 1
1SnV, 100	49 ± 3	55 ± 1	39 ± 2	52 ± 2	68 ± 1	55 ± 1
2SnV, 100	68 ± 3	54 ± 1	48 ± 2	71 ± 2	67 ± 2	51 ± 1

[a]Sx run: ϕ = 700 MeV.

needed in order to determine more specific constraints on how solar and volcanic changes each might have contributed to the observed climate changes.

6. Beryllium-10 Response to Production and Climate Change

6.1. Solar Impacts

[23] In our simulations, climate changes resulting from reduced TSI affect the atmospheric transport of ^{10}Be in some respects, however changes in ^{10}Be deposition and concentration at the surface tend to be relatively small. *Land and Feichter* [2003] found that the transformed Eulerian mean meridional circulation in the stratosphere increases in a warmer climate, and that stratospheric ^{10}Be concentrations tend to decrease. Consistently, in our solar minimum runs, we find that transformed stream function values decrease by 5–35% in the NH stratosphere relative to the solar maximum scenario. As a result of the changes in stratospheric circulation, stratospheric ^{10}Be concentrations increase up to 7%.

[24] In both hemispheres, colder temperatures at the surface and increased high-latitude sea level pressure lead to reduced precipitation over Greenland and Antarctica, which allows tropospheric concentrations of ^{10}Be over these areas to increase. Dry deposition of ^{10}Be at high latitudes increases accordingly, however because of the relative predominance of ^{10}Be in wet deposition, the impact of climate changes on total ^{10}Be deposition (wet plus dry) is negligible. (In contrast, *Heikkilä et al.* [2008] show depositional changes in ^{10}Be over Greenland that range from 20 to 200%, however their simulations feature a global cooling of 0.7°C and a change in ϕ from 700 MeV to 200 MeV and so are not strictly comparable.) The limited impact of solar forcing on our ^{10}Be deposition is illustrated in Figure 2, which shows the zonal average percent increase in total ^{10}Be deposition for the four solar minimum runs relative to the solar maximum run (results are shown for ϕ = 500 MeV, which closely resemble both the results for ϕ = 100 MeV and the runs with volcanic forcing.) The higher levels of ^{10}Be deposition at midlatitudes and high latitudes reflect the fact that ^{10}Be production is greater at those latitudes, and also indicate the degree to which ^{10}Be deposition at higher latitudes is representative of the global average production rate (high levels of atmospheric mixing) or the local production rate (limited atmospheric mixing). The polar enhancement in ^{10}Be deposition relative to other latitudes (calculated as the percent change in high-latitude deposition divided by the percent change in solar-related global average production) is approximately 1.3, similar to previously modeled and estimated values [*Field et al.*, 2006; *Bard et al.*, 1997].

[25] Similarly, Figure 3 shows the percent change in ^{10}Be snow concentration over Greenland (due only to TSI-related climate changes, not to production change) for the 1Sn, 2Sn, 3Sn and 4Sn scenarios relative to the Sx run (results are shown for ϕ = 100 MeV, which closely resemble the results for ϕ = 500 MeV (not shown)). Excepting the anomalous behavior of a few of the Greenland grid boxes (likely due to limitations in the model's topographical and spatial resolution), there is a consistent pattern of increased ^{10}Be snow concentration over northeast Greenland. However, despite the progressive cooling evident in Table 2, there is no clear trend in the pattern or magnitude of the concentration changes as TSI decreases. When data are grouped instead by the amount of production change (ϕ = 500 MeV and ϕ = 100 MeV) rather than by the amount of TSI change, a clear distinction emerges. Table 3 shows simulated changes in ^{10}Be snow concentration values at six coring sites for the two different levels of production change. Data are shown for 1Sn-4Sn climate forcings, and also for the case of no change in TSI (0Sn). The concentration changes for ϕ = 500 MeV and ϕ = 100 MeV are closely clustered around low and high values respectively, with no overlap between concentration values for the two different levels of production. Changes in production therefore have a much more robust impact on ^{10}Be snow concentration than do TSI-related climate changes for this range of forcing.

[26] In order to quantify the relative importance of production changes and climate changes, we used multiple linear regression of modeled ^{10}Be concentration with respect to ϕ changes and TSI forcing for the six ice-core locations. The impacts of production change and climate change were only both significant at one location (Summit); at all other locations, only production change had a significant impact on ^{10}Be concentration. When we performed the same analysis on all Greenland locations collectively, climate and production both were significant over Greenland, with ^{10}Be concentration changing about 9% per 100 MeV change in ϕ and 1.3% for each solar cycle of TSI change. When we analyzed both Antarctic locations, only production

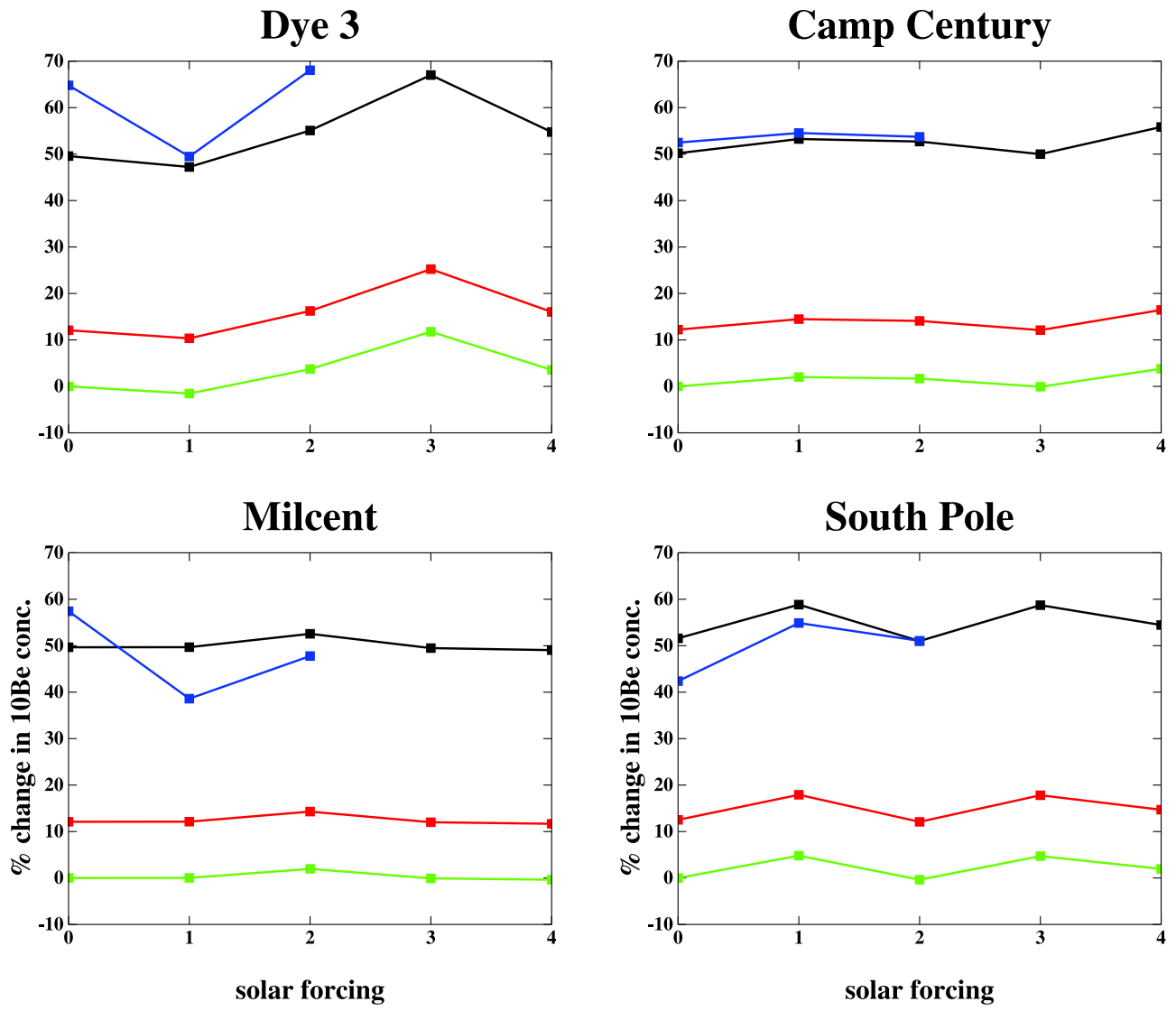

Figure 4. Percent change in modeled ^{10}Be snow concentration relative to the Sx run for different ice-core locations. Black line shows data for ϕ = 100 MeV; red line shows data for ϕ = 500 MeV; green line shows data for ϕ = 700 MeV; and blue line shows data for ϕ = 100 MeV with volcanic forcing.

was significant, again with approximately a 9% change in ^{10}Be concentration per 100 MeV change in ϕ.

[27] Figure 4 summarizes the effects of both production change and TSI-related climate change for four ice-core locations. Each line shows the percent change in ^{10}Be snow concentration relative to the control run for a given value of ϕ. For the ϕ = 700 MeV data, the model was forced with TSI changes while ^{10}Be production was kept constant. The plots show how concentration is affected at each level of solar forcing and also for the case of no solar forcing (only production changes). The changes in concentration for each given value of ϕ are clear and consistent from location to location: for each plot, ^{10}Be snow concentration for ϕ = 500 MeV is about 11% greater than the level for ϕ = 700 MeV, and the level for ϕ = 100 MeV is about 50% greater. However there are no clear trends associated with the effects of solar-related climate change, which in almost all cases are relatively small and not necessarily monotonic.

6.2. Volcanic Impacts

[28] The additional impact of volcanic aerosol forcing on simulated ^{10}Be is very small compared to the solar-related climate effects: results for the 0SnV, 1SnV and 2SnV runs differ little from 1Sn and 2Sn runs. The reductions in transformed stream function values closely resemble the changes in the simulations with only solar forcing; the increases in atmospheric ^{10}Be concentrations are similar as well (9%). Zonal changes in wet, dry and total ^{10}Be deposition, as mentioned in section 6.1, are generally the same as for the solar-forcing runs, with negligible changes in total deposition regardless of the degree of TSI forcing. Similarly, although there are consistent increases in ^{10}Be snow concentration changes over northeast Greenland (Figure 3), there is no clear trend associated with the magnitude of the applied forcing.

[29] Figure 4 compares ^{10}Be snow concentration changes for the runs with additional volcanic forcing (blue line) to the runs with only solar forcing. While the relative changes

Table 4. Observed ^{10}Be Snow Concentration, Percent Change During the Maunder Minimum (1645–1715)[a]

Location	1650–1700 Versus 1550–1600	MM Versus 70-Year Average	MM Versus Long-Term Average
Dye 3	10 ± 6	25 ± 5	12 ± 4
Camp Century	36 ± 14	46 ± 12	53 ± 9
Milcent	47 ± 14	41 ± 10	30 ± 6
South Pole	5 ± 7	30 ± 7	11 ± 5

[a]For Dye 3, Milcent, and South Pole, the 70-year reference period is 1730–1800. For Camp Century, the reference period is 1317–1396. Estimates of the uncertainty in the mean are shown when possible. Data are from *Beer et al.* [1990] (Dye 3), *Beer et al.* [1988] (Camp Century), *Beer et al.* [1983] (Milcent), and *Raisbeck and Yiou* [2004] (South Pole).

in snow concentration are basically the same for the different levels of production change in the runs with only solar forcing, the volcanic runs follow different patterns, resulting in ^{10}Be snow concentrations that may be either higher or lower than the concentrations in the runs with solar forcing alone. For Dye 3, all the ^{10}Be concentration values associated with the volcanically forced runs are higher than the ϕ = 100 MeV solar-forced values. For South Pole and Milcent, the values for the runs with volcanic forcing are mostly lower, while at Camp Century, the values for the volcanic runs are nearly the same as the values for the runs with only solar forcing. Overall, these results suggest that the simulated effects of combined volcanic and solar forcings do not have a clear signature on large spatial scales. This effect can also be seen in Table 3 if one compares the volcanic data with the solar data for ϕ = 100 MeV. At four of the six locations, the snow concentration values for the volcanic runs either contain outliers that are exceptionally low or high relative to the solar runs (such as the 39% value for 1SnV at Milcent or the 71% value for 2SnV at Summit), or, as in the case of Taylor Dome, the volcanic concentrations are all larger than the corresponding solar-only values. It therefore seems possible that for the degree of forcing simulated here, volcanic-related climate effects can potentially have an impact on multidecadal ^{10}Be snow concentrations, which may make it difficult to determine the concomitant level of TSI change or production change.

7. Comparison With ^{10}Be Observations

[30] How can these results be used to interpret the observed ^{10}Be changes during the MM? Considering the tracer's relatively small response to simulated climate impacts, our results confirm that increased ^{10}Be concentrations during the MM are largely the result of changes in solar magnetic field strength and attendant cosmic ray modulation. That being said, what was the likely magnitude of that production change? In order to compare our modeled results with the ice-core data, we first need to determine the observed change in ^{10}Be snow concentrations. However given the quality of the observations, there is some ambiguity in choosing a method for making such a calculation. Table 4 shows three ways of estimating the percent change in ^{10}Be snow concentration (relative to specific baselines) for four different ice-core locations. The concentration changes vary depending on whether the MM values (1) are considered as a 50-year period and compared to the 50-year period 100 years prior, (2) are compared to a subset of the time series that has the same duration as the MM (approximately 70 years) but does not occur during (or has relatively little overlap with) other prolonged solar minima, or (3) are compared to the entire time series (which includes the effects of other Grand Minima [*McCracken et al.*, 2004]).

[31] We also consider a fourth method which was used by *McCracken et al.* [2004] to estimate ϕ during the MM. The authors used data from Dye 3 and South Pole, and at each location took the average of the highest 22-year means for ^{10}Be snow concentration during both the Maunder and Spoerer (approximately 1420–1540 A.D.) minima. (In the case of the South Pole data, the highest 22-year average during the Oort minimum (about 1050 A.D.) was also used). If we perform the same calculation and compare the resulting ^{10}Be concentrations to the 70-year reference period (method 2), the changes in concentration at South Pole and Dye 3 are about 52 ± 12% and 49 ± 8% respectively, resulting in an average change of 51 ± 15%.

[32] With these different estimates, we can compare the production-related ^{10}Be changes from the model in Table 3 to the observed changes in Table 4 to see what degree of ϕ change best matches the observations. This comparison is shown in Figure 5. In each of the four plots, the thick solid line shows the modeled change in ^{10}Be regressed against different changes in ϕ (the modeled values from Table 3 appear as solid squares for $\Delta\phi$ values of 200 MeV (for the ϕ = 500 MeV runs) and 600 MeV (for the ϕ = 100 MeV runs)). The results show the lack of a strong climate signal, with observed percent concentration change values ranging widely depending on location and also on which method of estimating the observed ^{10}Be change is used. For the concentration change estimates based on comparing 1650–1700 with 1550–1600 (method 1), the implied changes in ϕ range from 84 MeV (at South Pole) to 513 ± 228 MeV (at Milcent). For method 3 (MM versus the long-term mean of the time series), the estimated ϕ changes range from about 152 ± 85 MeV (Dye 3) to 611 ± 193 MeV (Camp Century).

[33] As mentioned earlier, *McCracken et al.* [2004] have estimated that ϕ = 84 ± 30 MeV during the MM, or rather that a change in ϕ of about 616 MeV took place relative to the approximate present-day average value of ϕ = 700. This $\Delta\phi$ = 616 MeV is larger than all but one of our estimated ϕ values. However if we recalculate our estimates on the basis of the 22-year South Pole and Dye 3 averages described earlier, the change in ϕ increases significantly. Depending on which location we use, the change in ϕ ranges from 543 to 572 MeV. While the relationship in this paper between ϕ and ^{10}Be concentration is based on the modeled changes in ^{10}Be at different ice-core locations, from *McCracken et al.* [2004] the same relationship is determined from the flux function described by *Webber and Higbie* [2003] as well as the atmospheric mixing model discussed by *McCracken* [2004]. Despite the differences between these two methodologies, the $\Delta\phi$ that we obtain are slightly smaller but comparable to those estimated by *McCracken et al.* [2004].

[34] Part of the explanation for the discrepancies between our MM ϕ estimates and that of *McCracken et al.* [2004]

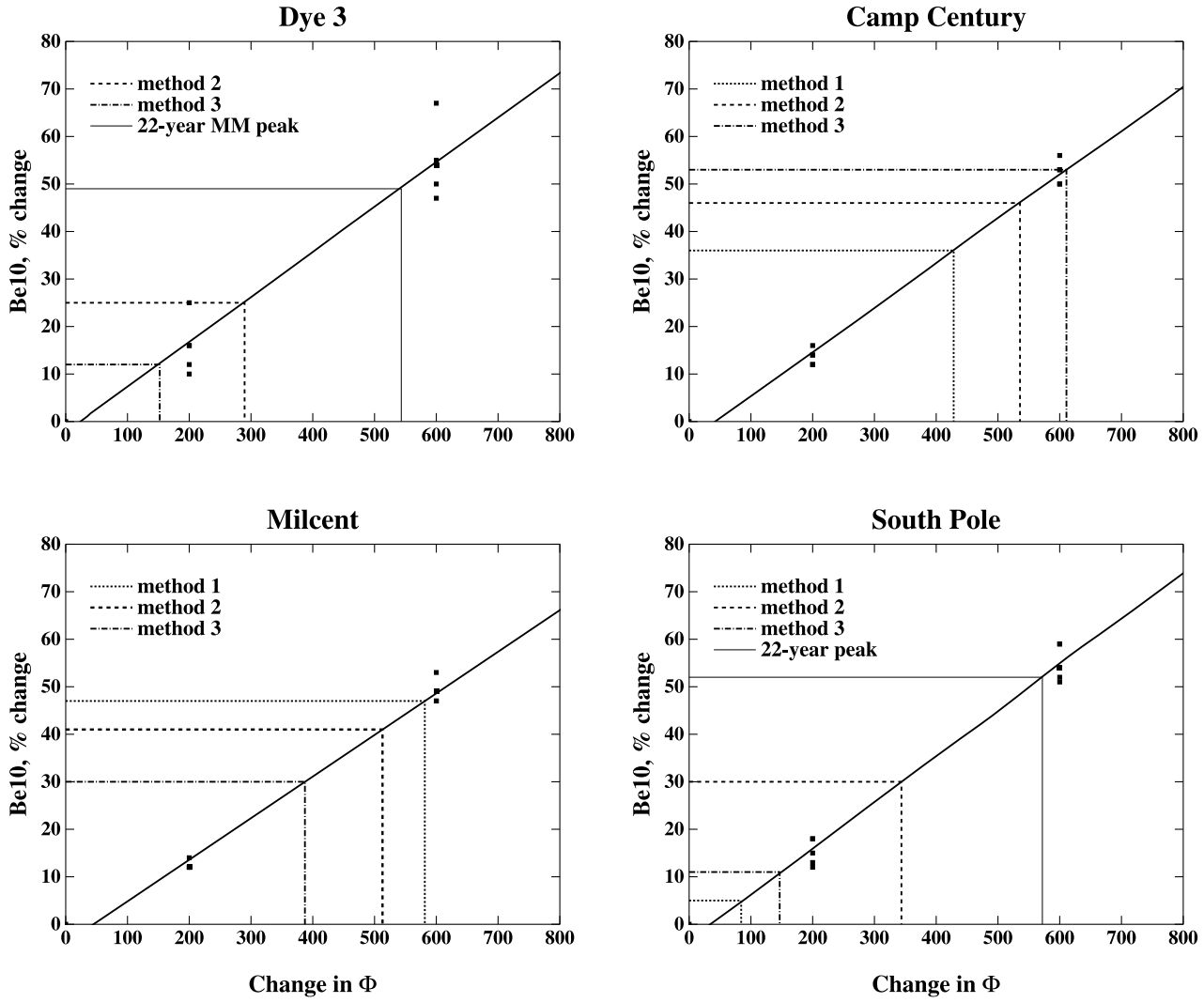

Figure 5. Comparison between the percent changes in observed MM ^{10}Be snow concentration for the different methods described in section 7 (dotted lines) and modeled ^{10}Be concentration changes (solid squares). The solid line shows the modeled ^{10}Be snow concentrations regressed against the associated change in ϕ. Key to observed changes in ^{10}Be snow concentration: 1 = 1650–1700 versus 1550–1600; 2 = MM versus 70-year mean, 3 = MM versus long-term mean (see Table 4). The 22-year value for Dye 3 is as described in section 7. The corresponding changes in ϕ can be read off the verticals.

may be differences in the amount of atmospheric mixing assumed by *McCracken et al.* [2004] compared to the amount of mixing in ModelE. As mentioned in section 6.1, in our simulations the ratio of the percent change in polar ^{10}Be deposition to the percent change in global average deposition is approximately 1.3, which implies a greater degree of atmospheric mixing that used by *McCracken et al.* [2004]. If the *McCracken et al.* [2004] calculations were repeated allowing for more mixing, it is likely that the resulting change in ϕ would be smaller and closer to more of our larger estimates.

[35] Another part of the difference between the ϕ estimates may be related to climate effects. *Horiuchi et al.* [2008], *Bard et al.* [2007] and *Muscheler et al.* [2007] have highlighted some of these concerns, particularly those relating to geographical and temporal variability of snow accumulation, and the effects of that variability on ^{10}Be ice core records. *Luterbacher et al.* [2004], *Jones et al.* [1998], and *Briffa et al.* [2001] have shown that the late 1600s and early 1700s were some of the coldest years of the MM, particularly in the NH and Europe. It is possible that these colder temperatures might have led to reduced precipitation around Greenland, resulting in higher ^{10}Be concentrations in the Dye 3 record for those years. Such an outcome would be similar to the findings discussed by *Field et al.* [2006], in which it was shown that significant reductions in ^{10}Be snow concentration can be caused by climate forcings alone (with no changes in cosmogenic production levels). As mentioned earlier, we see reduced accumulation in the experiments described here, but no consistent changes in ^{10}Be snow concentration relative to the degree of solar forcing. Nevertheless, even relatively modest amounts of climate variability, such as those shown in the plots for Camp Century and Milcent in Figure 5, could lead to a difference

of as much as 50 MeV in estimating the potential MM ϕ change. Also, although the relationship between ϕ and sunspots is still incomplete, the fact that sunspot counts for 1690–1715 were about the same or slightly higher than the counts during the rest of the MM suggests the possibility that local climate changes rather than production changes might have been partially responsible for the high ^{10}Be concentrations at Dye 3, which, in turn, might lead one to calculate a larger change in ϕ than what might have been inferred in the absence of climate effects.

[36] We see similar climate impacts in the analysis of our runs including enhanced volcanism. The results for Dye 3 in Figure 4 show that, on average, volcanic-related climate effects (blue line) lead to ^{10}Be concentration changes that are about 10% higher than those for equivalent runs with no volcanic effects. While this enhancement of the change in modeled ^{10}Be concentration is not statistically significant, it suggests the possibility that the effects of volcanic aerosols may have led to higher ^{10}Be concentrations at Dye 3 during the late MM. Elsewhere, however, such as in the 1SnV run at Milcent (39%) and in the 2SnV run at Summit (71%), the volcanic- and solar-forced changes in ^{10}Be concentration can be either notably reduced or enhanced relative to the simulations forced with TSI changes alone. It is possible that the model might have a different response to intermittent volcanism rather than the constant, sustained, low-level volcanic forcing that we used in these simulations. That being said, our results suggest that longer simulations are needed in order to clearly distinguish the effects of volcanic forcing from the weather noise.

[37] In addition to the ambiguities surrounding the methods for calculating MM ^{10}Be concentration changes and also the potential effects of climate change during that time, other factors exist that may have contributed to the uncertainties of our results. Regarding the observations, there is a fair amount of site-to-site variability in the changes we have estimated from the ^{10}Be concentration data. Local climate effects on Greenland are probably one of the main causes of the observed variability [*Mosley-Thompson et al.*, 2001]. Additionally, ice-core dating errors could potentially reduce the agreement between observed changes from site to site. Such errors can be as large as 2% over the past 1000 years but are often smaller and are less likely to be important contributors to the overall uncertainty [*Muscheler et al.*, 2007]. There are also issues relating to various characteristics of the experimental design, particularly the fact that estimates for the ^{10}Be production rate vary by as much as a factor of 2 [*Lal and Peters*, 1967; *Oeschger et al.*, 1969; *O'Brien et al.*, 1978; *Masarik and Reedy*, 1995; *Masarik and Beer*, 1999]. However, results here have been reported in terms of percent change from the control run, which should reduce the potential effect of errors in the magnitude of ^{10}Be production.

[38] Concerning the GCM itself, there are other considerations such as uncertainties relating to the model's climate sensitivity, which we have tried to address by performing simulations using a range of climate forcings. There are also uncertainties in the degree of TSI change and volcanic aerosol forcing during the MM. Another potential issue is the model's ability to simulate the general climate over Greenland and Antarctica. The quality of model results in these areas has been a focus of ongoing work, and we plan to continue this in the future by performing (1) simulations with higher spatial and vertical resolution, which would likely improve stratospheric dynamics and the consistency of grid-box-level performance, and (2) simulations spanning longer time periods, which should help clarify subtler changes such as those caused by volcanic aerosol forcing.

8. Conclusions

[39] Using the GISS ModelE GCM, it is possible to recreate the large-scale features of the MM climate using both solar forcings and volcanic forcings, or with solar forcings alone. If both volcanic and solar forcings are applied, the amount of solar forcing required to achieve a realistic amount of surface cooling is reduced. In the experiments with only conventional values of ^{10}Be production changes and solar forcing, the simulated ^{10}Be snow concentrations are influenced much more strongly by changes in production than by TSI-related changes in climate. Additional volcanic aerosol forcing does not have a straightforward impact on ^{10}Be over large spatial scales, however, further experiments are needed to better understand the full effects of this type of forcing. In comparing simulated and observed ^{10}Be snow concentration changes, the question of how best to define the observed MM change in ^{10}Be concentration remains ambiguous. The ϕ estimates based on the averages of methods 1, 2 and 3 give MM ϕ values ranging from approximately 280 to 395 MeV. If we look the average of the highest 22-year values for Dye 3 and South Pole, we get an estimate of $\phi = 142 \pm 150$ MeV. However the range of possible ϕ values inferred from time-averaging the other parts of the observed ^{10}Be record that could reasonably be considered representative of the MM suggests that additional analysis and better resolved data are necessary before a more decisive estimate can be made of how ϕ changed during the Maunder Minimum.

[40] **Acknowledgments.** We would like to thank to Jürg Beer and Josef Masarik for supplying ^{10}Be and ^{7}Be production functions, and David Rind for his help interpreting the dynamics. Support for this project was provided by NSF grant ATM-0317562. Christy Field also acknowledges support from the U.S. National Science Foundation through a Fellowship in the IGERT Joint Program in Applied Mathematics and Earth and Environmental Sciences at Columbia University.

References

Appenzeller, C., T. F. Stocker, and M. Anklin (1998), North Atlantic Oscillation dynamics recorded in Greenland ice cores, *Science*, *282*, 446–449.

Bard, E., G. M. Raisbeck, F. Yiou, and J. Jouzel (1997), Solar modulation of cosmogenic nuclide production over the last millennium: Comparison between ^{14}C and ^{10}Be records, *Earth Planet. Sci. Lett.*, *150*, 453–462.

Bard, E., J. Jouzel, and G. M. Raisbeck (2007), Comment on "Solar activity during the last 1000 yr inferred from radionuclide records" by Muscheler et al. (2007), *Quat. Sci. Rev.*, *26*, 2301–2304.

Beer, J., U. Siegenthaler, H. Oeschger, M. Andree, G. Bonani, M. Suter, W. Wölfli, R. Finkel, and C. C. Langway (1983), Temporal ^{10}Be variations, in *Contributions to the 18th International Cosmic Ray Conference*, edited by J. B. Blake et al., pp. 317–320, Adelaide Univ., Adelaide, South Aust., Australia.

Beer, J., et al. (1988), Use of ^{10}Be in polar ice to trace the 11-year cycle of solar activity, *Nature*, *331*, 675–679.

Beer, J., et al. (1990), Use of ^{10}Be in polar ice to trace the 11-year cycle of solar activity, *Nature*, *347*, 164–166.

Briffa, K. R. (2000), Annual climate variability in the Holocene: Interpreting the message of ancient trees, *Quat. Sci. Rev.*, *19*, 87–105.

Briffa, K., T. Osborn, F. Schweingruber, I. Harris, P. Jones, S. Shiyatov, and E. Vaganov (2001), Low-frequency temperature variations from a northern tree ring density network, *J. Geophys. Res.*, *106*, 2929–2941.

Chin, M., D. J. Jacob, G. M. Gardner, M. S. Foreman-Flower, P. A. Spiro, and D. L. Savoie (1996), A global three-dimensional model of tropospheric sulfate, *J. Geophys. Res.*, *101*, 18,667–18,690.

Crowley, T. J. (2000), Causes of climate change over the past 1000 years, *Science*, *289*, 270–277.

Crowley, T. J., and T. S. Lowery (2000), How warm was the medieval warm period?, *Ambio*, *29*, 51–54.

Crowley, T. J., G. Zielinski, B. Vinther, R. Udisti, K. Kreutz, J. Cole-Dai, and E. Castellano (2008), Volcanism and the Little Ice Age, *PAGES News*, *16*, 22–23.

Eddy, J. A. (1976), The Maunder Minimum, *Science*, *192*, 1189–1202.

Field, C. V., G. A. Schmidt, D. Koch, and C. Salyk (2006), Modeling production and climate-related impacts on ^{10}Be concentration in ice cores, *J. Geophys. Res.*, *111*, D15107, doi:10.1029/2005JD006410.

Foukal, P., C. Frohlich, H. Spruit, and T. M. L. Wigley (2006), Variations in solar luminosity and their effect on Earths climate, *Nature*, *443*, doi:10.1038/nature05072.

Free, M, and A. Robock (1999), Global warming in the context of the Little Ice Age, *J. Geophys. Res.*, *104*, 19,057–19,070.

Gillett, N. P., M. R. Allen, R. E. McDonald, C. A. Senior, D. T. Shindell, and G. A. Schmidt (2002), How linear is the Arctic Oscilliation response to greenhouse gases?, *J. Geophys. Res.*, *107*(D3), 4022, doi:10.1029/2001JD000589.

Gleeson, L. J., and W. I. Axford (1968), Solar modulation of galactic cosmic rays, *Astrophys. J.*, *154*, 1011–1018.

Haigh, J. D. (1996), The impact of solar variability on climate, *Science*, *272*, 981–984.

Heikkilä, U., J. Beer, and J. Feichter (2008), Modeling cosmogenic radionuclides ^{10}Be and ^{7}Be during the Maunder Minimum using the ECHAM5-HAM General Circulation Model, *Atmos. Chem. Phys.*, *7*, 2797–2809.

Horiuchi, K., T. Uchida, Y. Sakamoto, A. Ohta, H. Matsuzaki, Y. Shibata, and H. Motoyama (2008), Ice core record of ^{10}Be over the past millennium from Dome Fuji, Antarctica: A new proxy record of past solar activity and a powerful tool for stratigraphic dating, *Quat. Geochronol.*, *3*, 253–261.

Hoyt, D. V., and K. H. Schatten (1993), A discussion of plausible solar irradiance variations, 1700–1992, *J. Geophy. Res.*, *98*, 18,895–18,906.

Hoyt, D. V., and K. H. Schatten (1998), Group sunspot numbers: A new solar activity reconstruction, *Sol. Phys.*, *179*, 189–219.

Jones, P. D., and M. E. Mann (2004), Climate over past millennia, *Rev. Geophys.*, *42*, RG2002, doi:10.1029/2003RG000143.

Jones, P. D., K. R. Briffa, T. P. Barnett, and S. F. B. Tett (1998), High-resolution paleoclimatic records fo rhte last millennnium: Interpretation, integration and comparison with General Circulation Model control-run temperatures, *Holocene*, *8*, 455–471.

Koch, D., and D. Rind (1998), Beryllium 10/beryllium 7 as a tracer of stratospheric transport, *J. Geophy. Res.*, *103*, 3907–3917.

Koch, D., G. A. Schmidt, and C. V. Field (2006), Sulfur, sea salt and radionuclide aerosols in GISS modelE, *J. Geophys. Res.*, *111*, D06206, doi:10.1029/2004JD005550.

Lal, D., and B. Peters (1967), Cosmic ray produced radioactivity on the Earth, *Handb. Phys.*, *46*, 551–612.

Land, C., and J. Feichter (2003), Stratosphere-troposphere exchange in a changing climate simulated with the general circulation model MAEC-HAM4, *J. Geophys. Res.*, *108*(D12), 8523, doi:10.1029/2002JD002543.

Langematz, U., A. Claussnitzer, K. Matthes, and M. Kunze (2005), The climate during the Maunder Minimum: A simulation with the Freie Universitat Berlin Climate Middle Atmosphere Model (FUB-CMAM), *J. Atmos. Sol. Terr. Phys.*, *67*, 55–69.

Lean, J. (1994), Solar forcing of global change, in *The Solar Engine and Its Influence on Terrestrial Atmosphere and Climate*, *NATO ASI Ser.*, vol. 25, pp. 163–184, Springer, New York.

Lean, J. (2000), Evolution of the Suns spectral irradiance since the Maunder Minimum, *Geophys. Res. Lett.*, *27*, 2425–2428.

Lean, J., J. Beer, and R. Bradley (1995), Reconstruction of solar irradiance since 1610: Implications for climate change, *Geophys. Res. Lett.*, *22*, 3195–3198.

Lean, J. L., Y.-M. Wang, and J. N. R. Sheeley (2002), The effect of increasing solar activity on the Suns total and open magnetic flux during multiple cycles: Implications for solar forcing of climate, *Geophys. Res. Lett.*, *29*(24), 2224, doi:10.1029/2002GL015880.

LeGrande, A. N., G. A. Schmidt, D. T. Shindell, C. V. Field, R. L. Miller, D. M. Koch, G. Faluvegi, and G. Hoffmann (2006), Consistent simulations of multiple proxy responses to an abrupt climate change event, *Proc. Natl. Acad. Sci. U. S. A.*, *103*, 837–842, doi:10.1073pnas.0510095103.

Luterbacher, J., D. Dietrich, E. Xoplaki, M. Grosjean, and H. Wanner (2004), European seasonal and annual temperature variability, trends, and extremes since 1500, *Science*, *303*, 1499–1503.

Mann, M. E., R. S. Bradley, and M. K. Hughes (1999), Northern Hemisphere temperatures during past millenium: Inferences, uncertainties and limitations, *Geophys. Res. Lett.*, *26*, 759–762.

Masarik, J., and J. Beer (1999), Simulation of particle fluxes and cosmogenic nuclide production in the Earths atmosphere, *J. Geophys. Res.*, *104*, 12,099–12,111.

Masarik, J., and R. C. Reedy (1995), Terrestrial cosmogenic-nuclide production systematic calculated from numerical simulations, *Earth Planet. Sci. Lett.*, *136*, 381–395.

McCracken, K. G. (2004), Geomagnetic and atmospheric effects upon the cosmogenic ^{10}Be observed in polar ice, *J. Geophys. Res.*, *109*, A04101, doi:10.1029/2003JA010060.

McCracken, K. G., F. B. McDonald, J. Beer, G. Raisbeck, and F. Yiou (2004), A phenomenological study of the long-term cosmic ray modulation 850–1958 AD, *J. Geophys. Res.*, *109*, A12103, doi:10.1029/2004JA010685.

McHargue, L. R., and P. E. Damon (1991), The global beryllium 10 cycle, *Rev. Geophys.*, *29*, 141–158.

Miller, R. L., G. A. Schmidt, and D. T. Shindell (2006), Forced annular variations in the 20th century Intergovernmental Panel on Climate Change Fourth Assessment Report models, *J. Geophys. Res.*, *111*, D18101, doi:10.1029/2005JD006323.

Mosley-Thompson, E., J. R. McConnell, R. C. Bales, Z. Li, P.-N. Lin, K. Steffen, L. G. Thompson, R. Edwards, and D. Bathke (2001), Local to regional-scale variability of annual net accumulation on the Greenland ice sheet from PARCA cores, *J. Geophys. Res.*, *106*, 33,839–33,851.

Muscheler, R., F. Joos, J. Beer, S. A. Muller, M. Vonmoos, and I. Snowball (2007), Solar activity during the last 1000 yr inferred from radionuclide records, *Quat. Sci. Rev.*, *26*, 82–97, doi:10.1016/j.quascirev.2006.07.012.

O'Brien, K., H. A. Sandmeier, G. Hansen, and J. E. Campbell (1978), Cosmic-ray induced neutron background sources and fluxes for geometries of air over water, ground, iron, and aluminum, *J. Geophys. Res.*, *83*, 114–120.

Oeschger, H., J. Houtermann, H. Loosli, and M. Wahlen (1969), The constancy of cosmic radiation from isotope studies in meteorites and on the Earth, in *Radiocarbon Variations and Absolute Chronology*, edited by I. Olsen, pp. 471–498, John Wiley, Hoboken, N. J.

Overpeck, J., et al. (2004), Arctic environmental changes of the last four centuries, *Science*, *278*, 1251–1256.

Palmer, M. A., L. J. Gray, M. R. Allen, and W. A. Norton (2004), Solar forcing of climate: Model results, *Adv. Space Res.*, *34*, 343–348.

Radick, R. R., G. W. Lockwood, and S. L. Baliunas (1990), Stellar activity and brightness variations: A glimpse at the Suns history, *Science*, *247*, 39–44.

Raisbeck, G. M., and F. Yiou (2004), Comment on "Millennium scale sunspot number reconstruction: Evidence for an unusually active Sun since the 1940s," *Phys. Rev. Lett.*, *92*, 199001.

Raisbeck, G. M., F. Yiou, J. Jouzel, J. R. Petit, N. O. Weiss, J. Alsop, and G. de Q. Robin (1990), ^{10}Be and δ 2H in polar ice cores as a probe of the solar variabilitys influence on climate, *Philos. Trans. R. Soc.*, *330*, 463–470.

Ribes, J. C., and E. Nesme-Ribes (1993), The solar sunspot cycle in the Maunder Minimum AD 1645 to AD 1715, *Astron. Astrophys.*, *276*, 549–563.

Rind, D., J. Lerner, K. Shah, and R. Suozzo (1999), Use of on-line tracers as a diagnostic tool in general circulation model development: 2. Transport between the troposphere and stratosphere, *J. Geophys. Res.*, *104*, 9151–9167.

Rind, D., J. Lerner, J. Jonas, and C. McLinden (2007), Effects of resolution and model physics on tracer transports in the NASA Goddard Institute for Space Studies general circulation models, *J. Geophys. Res.*, *112*, D09315, doi:10.1029/2006JD007476.

Rodrigo, F. S., D. Pozo-Vazquez, M. J. Esteban-Parra, and Y. Castro-Diez (2001), A reconstruction of the winter North Atlantic Oscillation index back to A. D. 1501 using documentary data from southern Spain, *J. Geophys. Res.*, *106*, 14,805–14,818.

Sato, M., J. Hansen, M. McCormick, and J. Pollack (1993), Stratospheric aerosol optical depths, 1850–1990, *J. Geophys. Res.*, *98*, 22,987–22,994.

Schmidt, G. A., et al. (2006), Present day atmospheric simulations using GISS Model-E: Comparison to in-situ, satellite and reanalysis data, *J. Clim.*, *19*, 153–192, doi:10.1175/JCLI3612.1.

Shindell, D. T., R. L. Miller, G. A. Schmidt, and L. Pandolfo (1999a), Simulation of recent northern winter climate trends by greenhouse-gas forcing, *Nature*, *399*, 452–455.

Shindell, D. T., D. Rind, N. Balachandran, J. Lean, and P. Lonergan (1999b), Solar cycle variability, ozone, and climate, *Science*, *284*, 305–308.

Shindell, D. T., G. A. Schmidt, M. E. Mann, D. Rind, and A. Waple (2001), Solar forcing of regional climate change during the Maunder Minimum, *Science*, *294*, 2149–2152.

Shindell, D. T., G. A. Schmidt, M. E. Mann, and G. Faluvegi (2004), Dynamic winter climate response to large tropical volcanic eruptions since 1600, *J. Geophys. Res.*, *109*, D05104, doi:10.1029/2003JD004151.

Shindell, D. T., G. Faluvegi, R. L. Miller, G. A. Schmidt, J. E. Hansen, and S. Sun (2006a), Solar and anthropogenic forcing of tropical hydrology, *Geophys. Res. Lett.*, *33*, L24706, doi:10.1029/2006GL027468.

Shindell, D. T., G. Faluvegi, N. Unger, E. Aguilar, G. A. Schmidt, D. M. Koch, S. E. Bauer, and R. L. Miller (2006b), Simulations of preindustrial, present-day, and 2100 conditions in the NASA GISS composition and climate model G-PUCCINI, *Atmos. Chem. Phys.*, *6*, 4427–4459.

Steinhilber, F., J. A. Abreu, and J. Beer (2008), Solar modulation during the Holocene, *Astrophys. Space Sci. Trans.*, *4*, 1–6.

Stuiver, M., and P. D. Quay (1980), Changes in atmospheric C-14 attributed to a variable Sun, *Science*, *207*, 11–19.

Vonmoos, M., J. Beer, and R. Muscheler (2006), Large variations in Holocene solar activity: Constraints from ^{10}Be in the greenland ice core project ice core, *J. Geophys. Res.*, *111*, A10105, doi:10.1029/2005JA011500.

Webber, W. R., and P. R. Higbie (2003), Production of cosmogenic Be nuclei in the Earths atmosphere by cosmic rays: Its dependence on solar modulation and the interstellar cosmic ray spectrum, *J. Geophys. Res.*, *108*(A9), 1355, doi:10.1029/2003JA009863.

Wesely, M. L., and B. B. Hicks (1977), Some factors that affect the deposition rates of sulfur dioxide and similar gases on vegetation, *J. Air Pollut. Control Assoc.*, *27*, 1110–1116.

Willson, R. C., and H. S. Hudson (1988), Solar luminosity variations in solar cycle 21, *Nature*, *332*, 95–97.

C. V. Field, G. A. Schmidt, and D. T. Shindell, NASA Goddard Institute for Space Studies, Columbia University, 2880 Broadway, New York, NY 10025, USA. (cfield@giss.nasa.gov)